River Flow 2010 - Dittrich, Koll, Aberle & Geisenhainer (eds) - © 2010 Bundesanstalt für Wasserbau ISBN 978-3-939230-00-7

The flow and turbulence structure at a rectangular bridge pier with a low angle of attack

W.Y. Chang
National Center for High Performance Computing, Hsinchu 30076, Taiwan

G. Constantinescu & S. Miyawaki
Civil and Environmental Engineering Department, The University of Iowa, Iowa City, Iowa, USA

W.F. Tsai & H.C. Lien
National Center for High Performance Computing, Hsinchu 30076, Taiwan

ABSTRACT: Detached Eddy Simulation (DES) is used to study the vortical structure of the flow around a high-aspect-ratio rectangular bridge pier with a small angle of attack. Though piers are generally designed to be closely aligned with the incoming flow at normal flow conditions, the angle of attack can increase significantly at flood conditions. This is particularly the case when a pier is situated near an abutment in a compound channel which is, in many cases, subject to varying flow orientations as the flow stage rises. Simulations are conducted with two angles of attack (0^0 and 15^0) at a channel Reynolds number of 2.4×10^5. The paper focuses on the dynamics of the large-scale coherent structures forming around the bridge pier and their role in controlling the sediment entrainment and transport mechanisms at conditions corresponding to the start of the scour process (flat-bed channel). Simulation results show that for these conditions the horseshoe vortex system plays a relatively minor role in the entrainment of sediment from the bed. At the start of the scour process, most of the sediment is entrained from the bed by the eddies shed inside the separated shear layers forming on the two sides of the rectangular pier and by the strongly accelerated flow on the outer side of these two shear layers.

Keywords: Numerical Simulations, Coherent Structures, Local Scour, Bridge Piers

1 INTRODUCTION

The dynamics of the large-scale coherent structures controls to a large degree the geomorphodynamic processes around bridge piers and bridge abutments (e.g., see Dargahi, 1990, Sumer & Fredsoe, 2002, Roulund et al., 2005, Fael et al., 2006, Dey & Raikar, 2007, Unger and Hager, 2007, Kirkil et al., 2008, Koken & Constantinescu, 2008a-b, 2009). The flow around large in-stream flow obstacles generates complex large-scale eddies (e.g., necklace vortices at the base of the obstacle that form due to the adverse pressure gradients induced by the presence of the obstacle, eddies convected toward the bed with the downflow parallel to the upstream face of the obstacle, vortex tubes inside the separated shear layers, large scale rollers shed in the wake of the obstacle) that are much stronger than the eddies associated with the sweep and ejection events observed in turbulent channel flows with smooth or rough beds. These coherent structures are responsible for most of the scouring and erosion of the river bed in the vicinity of the obstacle. Most of the research in this area was driven by the need to predict local scour around bridge piers and abutments because excessive scour can lead to the collapse of bridges (Melville, 1997, Sumer & Fredsoe, 2002).

Existing scour prediction methods do not sufficiently recognize all the processes at play during scour, in particular the role of the large-scale coherent structures. This is one of the main reasons why the existing, frequently used, prediction methods yield scour depth estimates that substantially exceed observed depths at obstructions (e.g., piers) of noncircular shape. This is particularly true for high-aspect-ratio rectangular bridge piers that are commonly used for small and large bridges. Overestimation of the scour depth becomes an increasingly unacceptable economic proposition for large bridges where these piers are used. The development of new scour prediction methods that incorporate more physics requires to understand the turbulence structure and the dynamics of the eddies controlling the sediment entrainment, transport and deposition during the scour process.

In the present study Detached Eddy Simulation (DES) is used to investigate the changes in the flow and turbulence structure with the angle of attack in the flow past a high-aspect-ratio rectangular pier mounted on a flat-bed channel at a channel Reynolds numbers defined with the incoming mean channel velocity, U, and the channel depth, H, of 2.4×10^5. The Reynolds number is high enough such that the flow structure and dynamics of the coherent structures are qualitatively similar to those observed at field conditions, at least in small to medium size rivers. Consistent with field conditions, the incoming flow in the simulations is fully turbulent and contains resolved turbulence. The base case (zero angle of attack, $\alpha=0^0$) corresponds to conditions close to normal conditions in the river, where the flow is approximately aligned with the major axis of the rectangular pier. The second simulation is conducted with an angle of attack of 15^0 corresponding to flood conditions, where, as a result of the increase in the free surface elevation and the flooding of the floodplain, the flow direction at the bridge crossing is expected to change. The angle of attack can increase considerably at flood conditions especially for braided channels or, over time, in meandering channels. As a result of the flow deflection, the pier skew angle relative to the main-channel axis is altered. Several experimental investigations (e.g., Laursen & Toch, 1956, Ettema et al., 1998) have documented the significant increase of the maximum scour depth with the skew angle for rectangular piers of varying aspect ratios. However, these investigations do not provide a detailed analysis of the changes in the flow structure and sediment entrainment mechanisms with the angle of attack at different stages of the scour process.

One should also mention that in a related DES study Kirkil & Constantinescu (2009) considered the extreme case, in which the incoming flow was perpendicular to the major axis of the pier, $\alpha=90^0$. For this case, the strengths of the HV system and of the large-scale vortex shedding behind the pier are expected to be the largest. Their investigation has shown important changes in the sediment entrainment mechanisms are present between piers of circular shape and rectangular piers at high angle of attack. However, very rarely the angle of attach at a rectangular bridge pier designed to be aligned with the flow at normal conditions increases to more than 40^0 as a result of changes in the flow conditions within the natural river reach. This motivates the need to investigate the flow structure and sediment entrainment mechanisms at piers with a small angle of attack.

2 NUMERICAL METHOD AND DESCRIPTION OF THE SIMULATIONS

Due to the large value of the Reynolds number, the present numerical simulations employ a non-zonal hybrid Reynolds-Averaged Navier Stokes (RANS) - Large Eddy Simulation (LES) method called Detached Eddy Simulation (e.g., see Travin et al., 2000, Constantinescu & Squires, 2004).

A general description of the DES code is given in Chang et al. (2007). The 3D incompressible Navier-Stokes equations are integrated using a fully-implicit fractional-step method. The governing equations are transformed to generalized curvilinear coordinates on a non-staggered grid. The convective terms in the momentum equations are discretized using a blend of fifth-order accurate upwind biased scheme and second-order central scheme. All other terms in the momentum and pressure-Poisson equations are approximated using second-order central differences. The discrete momentum (predictor step) and turbulence model equations are integrated in pseudo-time using alternate direction implicit (ADI) approximate factorization scheme. The Spalart-Allmaras one-equation model was used. Time integration in the DES code is done using a double time-stepping algorithm and local time stepping is used to accelerate the convergence at each physical time step. The time discretization is second order accurate.

The length scale is selected to be the flow depth (D=0.55 m). The mean velocity in the channel (U=0.45 m/s) is used as the velocity scale. The domain width in the simulation is 5.7D. These dimensions correspond to a set of experiments performed by Kirkil and Constantinescu (2009) with the same pier for an angle of attack of 90^0. The computational domain extends 5D upstream of the centroid of the pier. The length of the pier, L, was equal to the channel depth, D. Its thickness was 0.07D. The aspect ratio of the rectangular pier was close to 14.5. In the simulation with $\alpha=0^0$, the main axis of the pier was contained within the symmetry plane of the channel. The blockage ratio is less than 9% in the three simulations.

At the inflow section, turbulent inflow conditions corresponding to fully-developed turbulent channel flow are applied. The turbulence fluctuations are obtained from a periodic LES simulation in a straight channel. At the outflow, a convective boundary condition is used. The free surface is treated as a rigid lid which is justified as the channel Froude number is 0.2. All the walls are treated as no-slip smooth boundaries. The lateral boundaries were treated as symmetry (slip).

The computational domain was meshed using about 10 million cells. A minimum grid spacing of one wall unit was used in the wall normal direction. The grid spacing in the HV region was about 200 wall units. The origin of the system of coordinates is located at the center of the cylinder on the bottom surface with the x axis in the streamwise direction. The physical time step was 0.025D/U.

3 DISCUSSION OF FLOW PHYSICS

Figure 1 visualizes the mean (time-averaged) flow pattern using 3D streamlines launched in the near-bed region upstream of the pier. In the simulation with $\alpha=0^0$, on both sides of the pier, two small recirculation bubbles are observed close to the upstream edge of the pier, in between the separated shear layer and the lateral face, and behind the downstream face of the pier, in the near wake. The flow remains attached over most of the lateral faces of the pier.

In the simulation with $\alpha=15^0$ the flow remains attached over the whole length the left (relative to the incoming flow direction) lateral face of the pier. However a large recirculation bubble forms over the whole depth of the channel behind the lateral face situated on the right side of the pier. The bubble extends for some distance behind the pier and is laterally bordered by the two separated shear layers that originate at the upstream and downstream edges of the pier.

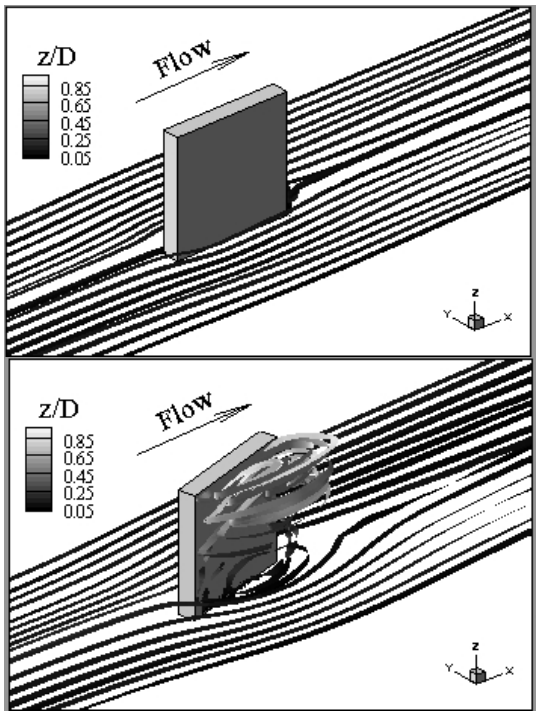

Figure 1. Visualization of the (time-averaged) mean flow around the pier in the simulations with $\alpha=00$ (top) and $\alpha=150$ (bottom) using 3D streamlines. The streamlines originate in the near-bed region upstream of the pier.

The position and extent of the two shear layers in the mean flow are visualized in Figure 2. This figure shows the distribution of the out-of-plane vorticity at mid-channel depth (z/D=0.5) and is representative of the distribution of the out-of-plane vorticity in horizontal planes over the whole depth of the channel. Some 3D effects are however present. A weak upwelling motion is present within the main separation bubble and the size of the bubble decreases as the bed surface is approached. This is also confirmed by examination of the trajectories of the 3D streamlines used to visualize the recirculation bubble in Fig. 2b.

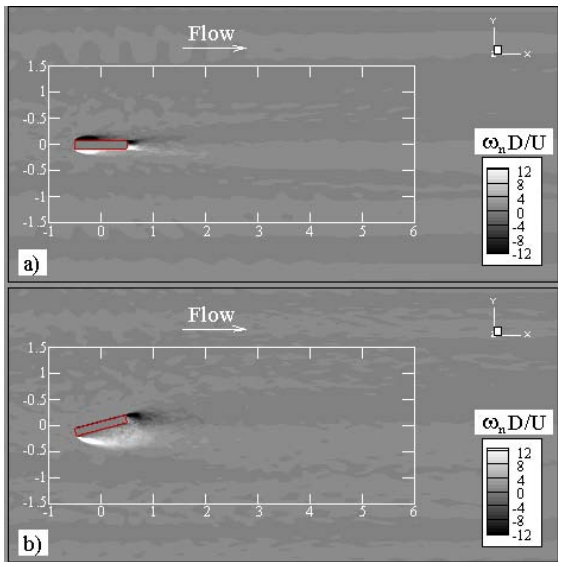

Figure 2. Distribution of the non-dimensional vertical vorticity in the mean flow (z/D=0.5) around the pier in the simulations with $\alpha=00$ (top) and $\alpha=150$ (bottom).

Figure 3 gives more details on the vortical content of the separated shear layers and near wake. As expected, at both angles of attack, the separated shear layers are populated by strong vortical eddies that are convected away from the edges of the pier where the shear layer originated. These eddies, which resemble vortex tubes whose axes are close to vertical, maintain their coherence in the near bed region, similar to the case when $\alpha=90^0$ that was investigated by Kirkil & Constantinescu (2009). Thus, their capacity to entrain sediment particles as they are convected away from the pier remains large, at least over the upstream part of the separated shear layers. Comparison of the instantaneous vorticity distributions in Figures 3a and 3b shows that the coherence and strength of the eddies are the largest for the shear layer on the right side of the pier in the case with $\alpha=15^0$. At times, some of the eddies convected inside this shear layer are entrained within the recirculation bubble behind the pier and can entrain sediment particles situated just behind the pier in a region where the bed friction velocity in the mean flow is very low.

The instantaneous vorticity distributions in Figure 3 also capture the large scale vortex shedding behind the pier. The passage of the rollers is another important mechanism for entrainment and transport of sediment particles downstream of the pier. Examination of the mean flow fields (e.g., see Figures 1, 2, 4) does not allow to capture, and even less to quantitatively analyze, these mechanisms. This shows the importance of analyzing not only the mean flow and turbulence structure but also the instantaneous flow fields (e.g., vorticity, bed friction velocity) to be able to describe the sediment entrainment and transport around a bluff body (e.g., bridge pier). This is because some of the large-scale coherent structures (e.g., rollers) playing an important role in the transport of sediment are not present in the mean flow fields.

Observe the undulatory shape of the near wake that contains patches of high vorticity distributed on the two sides of the symmetry plane of the channel. These patches containing high vorticity of positive and, respectively, negative sign correspond to the rollers that are shed at a close to constant frequency behind the pier. The strength of the rollers increases significantly between $\alpha=0^0$ and $\alpha=15^0$. This increase will continue monotonically until $\alpha=90^0$, though the rate of increase is expected to be much smaller at high angles of attack ($\alpha>40^0$).

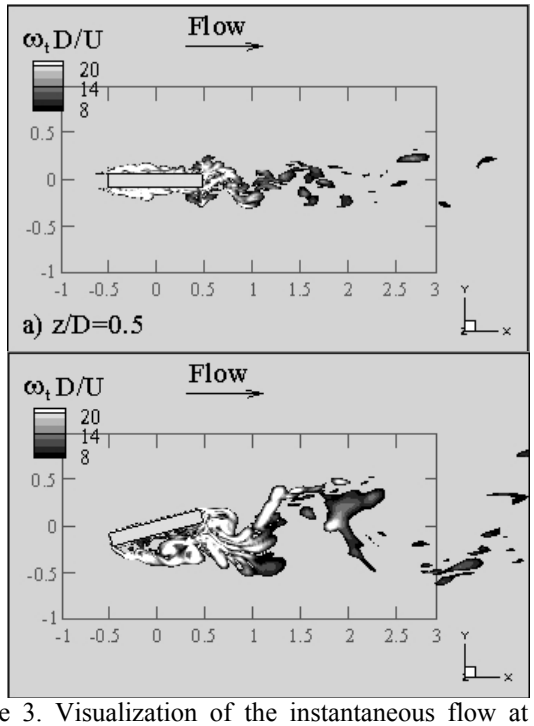

Figure 3. Visualization of the instantaneous flow at mid-depth level (z/D=0.5) around the pier in the simulations with $\alpha=00$ (top) and $\alpha=150$ (bottom) using non-dimensional vorticity magnitude contours.

The non-dimensional frequency expressed as a Strouhal number (St=fD/U) has increased from 0.153 for $\alpha=0^0$ to 0.211 for $\alpha=15^0$. The change in the blockage ratio was only 3.5%, thus its effect on St was not significant. Though the passage of the rollers at a higher frequency is expected to allow for more sediment entrainment by the rollers per unit time, the coherence of the rollers is much smaller in the simulation with $\alpha=0^0$. By contrast, in the simulation with $\alpha=15^0$ the amplification of the bed friction velocity beneath the rollers is significant and, equally important, the values of the bed friction velocity within these regions decay slowly as the rollers get away from the pier. This is qualitatively similar to what Kirkil & Constantinescu (2009) observed at much larger angles of attack ($\alpha=90^0$). Thus, a small increase of the angle of attack can result in a large increase of the capacity of the rollers shed in the wake to entrain and carry sediment over large distances behind the pier.

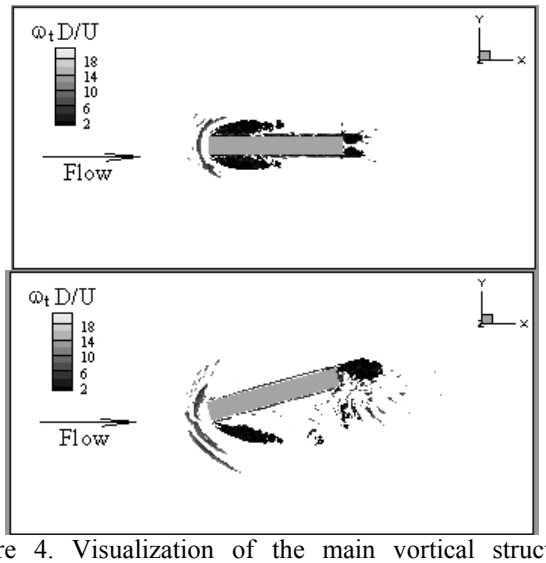

Figure 4. Visualization of the main vortical structures around the pier in the mean flow in the simulations with $\alpha=0^0$ (top) and $\alpha=15^0$ (bottom) using the Q criterion. The view is from above.

The Q criterion was used to visualize the coherent structures in the mean flow and instantaneous flow in Figures 4 and 5, respectively. In the mean flow, the Q criterion visualizes the separated shear layers and the necklace vortices part of the horseshoe vortex (HV) system. In the instantaneous flow, the Q criterion shows that the region behind the pier and the near wake is populated by a wide range of eddies. Interestingly, not all the dynamically important eddies have their axes oriented vertically as will be expected in the case of a very deep flow. Especially in the case when $\alpha=15^0$, the relatively high shallowness of the flow induces the presence of strong eddies whose axes are close to parallel to the bed. These eddies are predominantly present in the regions connecting two successively shed vortices. Such eddies were also observed at much higher angles of attack (see discussion in Kirkil & Constantinescu, 2009). The presence of such strong eddies in the vicinity of the bed can provide an additional mechanism for

the entrainment of the sediment from the bed in the near wake region.

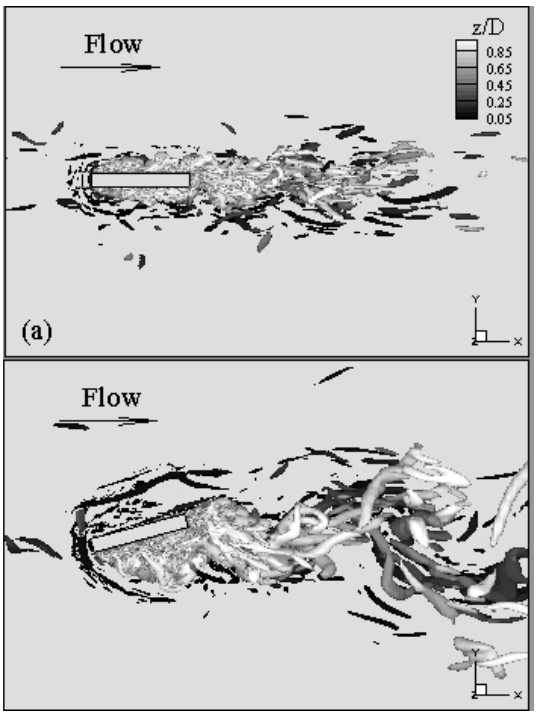

Figure 5. Visualization of the main vortical structures around the pier in the instantaneous flow in the simulations with α=00 (top) and α=150 (bottom) using the Q criterion. The view is from above.

The results in Figures 4a and 5a show that a HV system is present in the simulation with $\alpha=0^0$. In the mean flow, the HV system contains only one necklace vortex whose position is symmetric with respect to the symmetry axis of the channel in the spanwise direction. The legs of the necklace vortex are approximately parallel to the outer face of the shear layers forming at the two upstream edges of the pier. However, the legs extend only over a short distance past the upstream edges of the pier. In the simulation with $\alpha=15^0$ the structure of the HV system is more complex. Besides the main necklace vortex that is positioned close to the upstream tip of the pier, a second necklace is present on the side of the stronger shear layer. This vortex is situated upstream of the necklace vortex extending on both sides of the pier and has a strength that is comparable to that of the other necklace vortex. The cores of the two vortices are approximately parallel and their legs move slightly away from the outer face of the stronger shear layer.

The analysis of the coherent structures in Figures 5a and 5b show some interesting differences with the necklace vortices visualized in the mean flow fields in the two simulations. In the case with $\alpha=0^0$, the legs of the main necklace vortex in the instantaneous flow fields do not extend laterally over significantly larger distances compared to the mean flow. This changes dramatically in the case with $\alpha=15^0$ in which the legs of the main necklace vortices can extend, at times, even past the downstream end of the pier. Interestingly, this happens not only on the side of the stronger shear layer (right side of the pier) but also on the other side of the pier (left side). For example, the necklace vortex on the left side is stronger and extends further downstream compared to the one on the right side in Figure 5b. However, analysis of the instantaneous vorticity fields in vertical planes cutting through the cores of these necklace vortices shows that the circulation associated with these necklace eddies is relatively small, and their capacity to induce large bed friction velocities beneath them is reduced. By contrast, animations of the instantaneous flow fields in the simulation with $\alpha=0^0$ show that the main necklace vortex is relatively stable and, despite the small size of the core, its circulation is relatively high. As a result, at times the amplification of the bed friction velocity beneath the main necklace vortex is significant in the simulation with $\alpha=0^0$. Most of the events that result in a strong amplification of the strength of the circulation and the bed shear stress beneath the necklace vortex are associated with the convection of strong vortical eddies with the downflow that follows the upstream face of the pier. This amplification is comparable to the one observed beneath the separated shear layers. The stronger coherence of the HV system close to the tip of the pier in the simulation with $\alpha=0^0$ is also confirmed by comparison of the turbulent kinetic energy distributions in planes cutting through the upstream tip of the pier in the two simulations (not shown). The amplification of the turbulent kinetic energy in the HV region and within the downflow is about two times larger in the simulation with $\alpha=0^0$. Of course, this is expected to change as the angle of attack continues to increase past 15^0 and the strength of the adverse pressure gradients induced by the flow blockage by the left side of the pier becomes important.

The distributions of the bed friction velocity in the mean flow in Figure 6 confirm the fact that the capacity of the necklace vortices to entrain sediment is small at both angles of attack in the flat bed simulations. Still, the larger strength of the downflow in the simulation with $\alpha=0^0$ explains the relatively large amplification of the pressure root-mean-square (rms) fluctuations in the same simulation in Figure 7a. Such an amplification is not present in the case with $\alpha=15^0$ for the reasons discussed above.

In fact, examination of the instantaneous distributions of the bed friction velocity in both simulations shows that, at times, the levels of u_τ/U are comparable to those observed in the region associated with the separated shear layers. Thus, even

at conditions corresponding to the start of the scour process, scour is expected to occur beneath the HV system. However, as the period of time when the circulation of the main necklace vortices is high is relatively small compared to the period of time when the strength of these vortices is not sufficient to induce a large amplification of u_τ/U, the distribution of u_τ/U in the mean flow shows small values beneath the region associated with the HV system. This shows again the necessity to analyze the sediment entrainment mechanisms based not only on the mean flow quantities but also on the distribution of these quantities in the instantaneous flow fields. In both simulations, the regions where a large amplification of u_τ/U occurs in the instantaneous flow fields correspond to the necklace vortex situated the closest to the pier. In the case with $\alpha=15^0$, the amplification is significantly larger on the side of the stronger shear layer despite the fact that the legs of the necklace vortex can extend at considerable distances away from the tip of the pier on both sides.

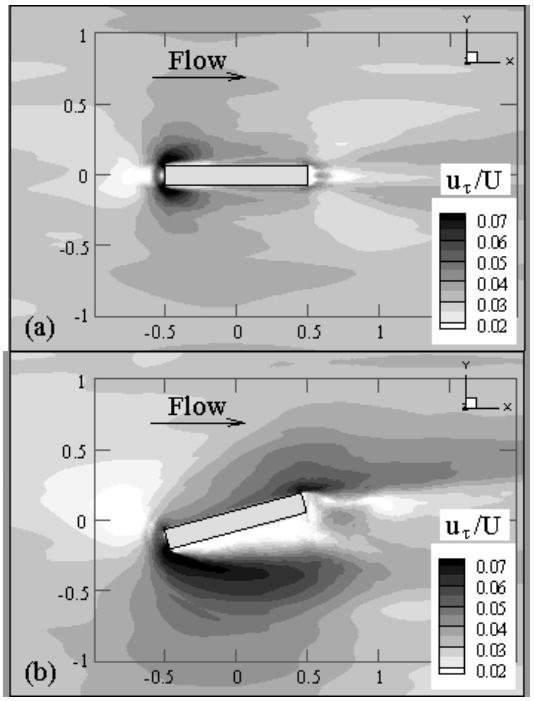

Figure 6. Distribution of the non-dimensional bed-friction velocity, in the mean flow in the simulations with $\alpha=00$ (top) and $\alpha=150$ (bottom).

However, the distributions of u_τ/U in Figure 6 show that most of the sediment is entrained from the bed beneath the shear layers and on their outer side where the incoming flow is accelerated as a result of the flow blockage induced by the pier. The fact that the regions of strong values of u_τ/U do not correspond exactly with the position of the separated shear layers can be observed from the comparison of the distributions of the vorticity and bed friction velocity in Figures 2 and 6, respectively. The regions of high vorticity magnitude are situated closer to the faces of the pier compared to the regions of high values of u_τ/U.

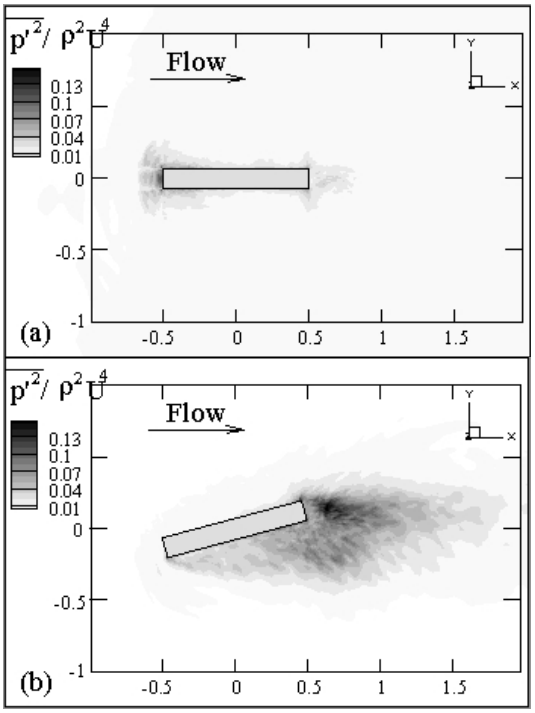

Figure 7. Distribution of the non-dimensional pressure rms fluctuations at the channel bottom in the simulations with $\alpha=00$ (top) and $\alpha=150$ (bottom).

The increase in the angle of attack from 0^0 to 15^0 resulted in an increase by about 6 times of the regions where $u_\tau/U>0.06$. Most of the increase takes place around the shear layer forming on the right side of the pier. Thus, during the initial stages of the scour process, one expects the scour hole around the pier to grow at a much faster rate in the simulation with a higher angle of attack. Moreover, the examination of the instantaneous distributions of the bed friction velocity in the simulation with $\alpha=0^0$ shows that patches of large values of u_τ/U are induced beneath the rollers that are convected away from the pier. The values of u_τ/U beneath the rollers in the region with $x/D<3$ (the pier occupies the region with $-0.45<x/D<0.45$) are comparable to those induced beneath the separated shear layers in the mean flow. Similar to the case of large angles of attack investigated by Kirkil & Constantinescu (2009), the rollers follow a trajectory that is approximately parallel to the symmetry plane ($y/D=0$) of the channel. Thus, the unsteady dynamics of the large scale eddies in the near wake can also induce sediment entrainment. The size of the region of large values of the bed friction velocity induced by the wake rollers is expected to increase monotonically with the angle of attack. Finally, one should mention that the bed friction velocity is small in the region situated beneath the recirculation bubble present in the case with $\alpha=15^0$. This means that sediment particles can easily deposit in these regions. However, this

is not likely to happen because of the weak upwelling motion of the mean flow within the recirculation bubble (see Figure 1b).

Besides the bed friction velocity, the pressure rms fluctuations in the near bed region is the other variable that can strongly affect the capacity of the flow to entrain sediment. Comparison of Figures 6 and 7 shows that, at both angles of attack, the distributions of the two variables are not similar. This is especially true in the simulation with $\alpha=15^0$ where the largest values of the pressure rms fluctuations occur on the inner side of the shear layer originating at the downstream end of the pier. The amplification appears to be triggered by the passage of the vortex tubes inside this shear layer. The levels of the pressure rms fluctuations are smaller by a factor of at least two in the shear layer originating at the upstream end of the pier. By contrast, the largest values of the bed friction velocity are observed on the outer side of the shear layer originating at the upstream end of the pier.

The main reason for the larger values of the pressure rms fluctuations in the region bordering the shear layer on the left side of the pier compared to the corresponding values on the right side is due to the fact that the flow favors the accumulation of the eddies shed in the left shear layer. This results into a stronger roller forming close to the downstream end of the pier. The other consequence is that the bed friction velocity values beneath the rollers detaching from the downstream end of the pier are, in average, larger than those induced by the rollers containing vorticity of opposite sign that form at the downstream end of the shear layer originating at the upstream end of the pier. Thus, despite the fact that the eddies convected in the shear layer originating on the right side of the pier are stronger, the rollers forming on the same side of the pier are weaker. Close to the downstream end of the pier, the pressure is reduced in the center of the rollers during their formation and increases once the roller leaves the region. The increase in the pressure rms fluctuations in that region is due the formation and detachment of the rollers near the downstream end of the pier. The fact that the rollers forming near the downstream end of the pier are stronger also explains the larger length of the region of relatively high values of the bed friction velocity on the left side of the pier in the mean flow (Figure 6b). This region is induced by the successive passage of the rollers detaching from the downstream end of the pier. These values are much smaller than the ones observed over the upstream part of the shear layer originating at the upstream end of the pier, but significantly larger than the ones recorded in the region situated beneath the path followed by the rollers forming on the right side of the pier. As the angle of attack start approaching 90^0 the differences in the distributions of the bed friction velcity and of the pressure rms fluctuations on the two sides of the pier are going to decrease.

4 SUMMARY AND CONCLUSIONS

The present paper provided a description of the main features of the flow field and turbulence structure in the vicinity of a high-aspect ratio rectangular pier at small angle of attack and a discussion of the roles of the dominant large-scale coherent structures and of their interactions in controlling the sediment entrainment phenomena around the bridge pier at conditions close to initiation of scour (flat bed channel) based on results of DES simulations. The angle of attack was varied between 0^0 and 15^0. This range of angles is typical for rectangular piers designed to be aligned with the flow at normal flow conditions. The Reynolds number in the simulations ($Re=2.4\times 10^5$) corresponds to the upper limit at which laboratory investigations are typically conducted.

Simulation results showed that a horseshoe vortex system is present at both $\alpha=0^0$ and $\alpha=15^0$, at conditions corresponding to the start of the scour process. In the simulation with $\alpha=0^0$, the lateral extent of the main necklace vortex and its diameter are relatively small but the amplification of the turbulence is relatively large (compared to the case of small but non-zero angles of attack) because the incoming flow decelerates strongly as it approaches the upstream face of the pier and the intensity of the downflow is large close to the junction line between the upstream face and the channel bed.

As the angle of attack increases to 15^0, the incoming flow is deflected on the two sides of the most upstream edge of the pier. This reduces the strength of the adverse pressure gradients and of the downflow around the most upstream part of the rectangular pier. The structure of the HV system becomes more complex (several necklace vortices are present), the mean diameter of the necklace vortices increases but the amplification of the turbulence within the HV region decreases compared to the case when $\alpha=0^0$. More importantly, in both simulations the amplification of the bed friction velocity beneath the necklace vortices is negligible compared to the one observed beneath the separated shear layers forming on the two sides of the rectangular pier.

The distribution of the pressure rms fluctuations at the bed shows that the downflow in the $\alpha=0^0$ case is strong enough to induce a significant amplification of this variable in front of the up-

stream face of the pier. By contrast, the amplification of the pressure rms fluctuations at the bed around the upstream part of the pier is negligible at small non-zero angles of attack. It is expected that at significantly larger angles of attack (e.g., see Kirkil and Constantinescu, 2009 who studied the case with $\alpha=90^0$) the amplification of the turbulence within the HV system region will be important and much larger than that observed at $\alpha=0^0$. As the angle of attack increases, the largest adverse pressure gradients are not generated in front of the small face of the pier but rather in front of the lateral face of the pier toward which the incoming flow is oriented. This also increases the intensity of the downflow and the strength of the necklace vortices. Thus, a recommendation for future study is to perform simulations over a larger range of angles of attack to get a better idea on the variation of the strength of the HV system with the angle of attack. A main conclusion is that for small non-zero angles of attack the capacity of the HV system to entrain sediment is smaller than that in the case when the flow is perfectly aligned with the major axis of the pier.

On the other hand, for the flat bed case the largest values of the bed friction velocity are observed beneath and especially on the outer sides of the separated shear layers where the incoming flow is strongly accelerated. The size of the region of relatively high bed friction velocity increases significantly with the angle of attack between $\alpha=0^0$and $\alpha=15^0$. Most of the amplification takes place close to the shear layer originating at the upstream edge of the pier. The fact that the largest values of the bed friction velocity are observed close to the position of the separated shear layers is consistent with experimental observations of local scour at circular and low-aspect-ratio rectangular piers that showed that the scour is initiated in the regions of high flow acceleration near the bed rather than beneath the main necklace vortex. Of course, as the angle of attack continues to increase one expects the bed friction velocity beneath and close to the shear layer originating at the downstream edge of the pier will start increasing significantly while that beneath and close to the shear layer originating at the upstream edge of the pier will grow at a much smaller rate or even decrease. This is because at $\alpha=90^0$, the amplification of the bed friction velocity around the shear layers forming on the two sides of the pier has to be identical because of the symmetry, similar to what was observed for $\alpha=0^0$.

As the angle of attack increases slightly past $\alpha=0^0$, the position of the region of high amplification of the pressure rms fluctuations moves from the front of the pier to a region situated slightly behind the downstream edge of the pier. Relatively high values of the pressure fluctuations at the bed are observed in the near wake region between the two separated shear layers. The region of significant amplification of the pressure fluctuations at the bed extends up to one length of the pier.

In conclusion, the present study shows that at the start of the scour process (flat bed channel), the horseshoe vortex system forming around a high-aspect-ratio pier at small angle of attack plays a relatively minor role in the entrainment of sediment from the bed. Most of the sediment is entrained from the bed by the eddies shed inside the separated shear layers forming on the two sides of the rectangular pier and by the strongly accelerated flow on the outer side of these two shear layers. To understand the mechanism responsible for sediment entrainment and transport around the pier one has to analyze not only the mean flow (e.g., vorticity, bed friction velocity) and turbulence structure (e.g., turbulent kinetic energy, pressure rms fluctuations) but also the dynamics of the large scale eddies in the instantaneous flow fields and the instantaneous distributions of relevant flow variables (e.g., vorticity, bed friction velocity).

ACKNOWLEDGEMENTS

Financial support from the National Science Council, Taiwan, under grant NSC 98-2625-M-492 -002 is highly appreciated. We are also grateful to the National Center for High-Performance Computing for computer time and facilities.

REFERENCES

Chang, K., Constantinescu, G., Park, S.O. 2007. Assessment of predictive capabilities of Detached Eddy Simulation to simulate flow and mass transport past open cavities. ASME J. Fluids Engineering, 129(11), 1372-1383.

Constantinescu, G., Squires, K.D. 2004. Numerical investigation of the flow over a sphere in the subcritical and supercritical regimes. Physics of Fluids, 16(5), 1449-1466. DOI 1070-6631/2004/16(5)/1449/18.

Dargahi, B. 1990. Controlling mechanism of local scouring. J. Hydraulic Engineering, 116 (10), 1197-1214.

Dey, S., Raikar, R.V. 2007. Characteristics of horseshoe vortex in developing scour holes at piers. J. Hydraulic Engineering, 133 (4), 399-413.

Ettema, R., Melville, B. W., Barkdoll, B. 1998. Scale effects in pier-scour experiments. J. Hydraulic Engineering, 124(6), 639-642.

Fael, C. M. S., Simarro-Grande, G., Martin-Vide, J. P.,, Cardoso, A. H. 2006. Local scour at vertical-wall abutments under clear water flow conditions. Water Resources Research, 42, W10408, doi:10.1029/2005WR004443.

Kirkil, G., Constantinescu, G., Ettema, R. 2009. DES investigation of turbulence and sediment transport at a circu-

lar pier with scour hole. J. Hydraulic Engineering, 135(11), 888-901.
Kirkil, G., Constantinescu, G. 2009. Nature of flow and turbulence structure around an in-stream vertical plate in a shallow channel and the implications for sediment erosion. Water Resources Research, 45, W06412, doi:10.1029/2008WR007363.
Koken, M., Constantinescu, G. 2008a. An investigation of the flow and scour mechanisms around isolated spur dikes in a shallow open channel. Part I. Conditions corresponding to the initiation of the erosion and deposition process. Water Resources Research, 44, W08406, doi:10.1029/2007WR006489.
Koken, M., Constantinescu, G. 2008b. An investigation of the flow and scour mechanisms around isolated spur dikes in a shallow open channel. Part II. Conditions corresponding to the final stages of the erosion and deposition process. Water Resources Research, 44, W08407, doi:10.1029/2007WR006491.
Koken, M., Constantinescu, G. 2009. An investigation of the dynamics of coherent structures in a turbulent channel flow with a vertical sidewall obstruction. Physics of Fluids, 21, 085104, DOI 10.1063/1.3207859.
Laursen, E.M., Toch, A. 1956. Scour around bridge piers and abutments. Bulletin No.4, Iowa Highways Research Board, Ames, Iowa, U.S.A.
Melville, B. W. 1997. Pier and abutment scour: integrated approach. J. Hydraulic Engineering, 123(2), 125-136.
Roulund, A., Sumer, B. M., Fredsoe, J., Michelsen, J. 2005. Numerical and experimental investigation of flow and scour around a circular pile. J. Fluid Mechanics, 534, 351-401.
Sumer, B. M., Fredsoe J. 2002. The mechanics of scour in the marine environment. World Scientific.
Travin, A., Shur, M., Strelets, M., Spalart, P.R. 2000. Physical and numerical upgrades in the detached-eddy simulation of complex turbulent flows." EUROMECH Colloquium on LES of Complex transitional and turbulent flows, Munich, Germany.
Unger, J., Hager, W.H. 2007. Downflow and horseshoe vortex characteristics of sediment embedded bridge piers. Experiments in Fluids, 42(1), 1-19 DOI 10.2007/s00348-006-0209-7.